

# High frequency, large displacement, and low power consumption piezoelectric translational actuator based on an oval loop shell

Taiho Yeom<sup>a</sup>, Terrence W. Simon<sup>a</sup>, Min Zhang<sup>a</sup>, Mark T. North<sup>b</sup>, Tianhong Cui<sup>a,\*</sup>

<sup>a</sup> Department of Mechanical Engineering, University of Minnesota, Minneapolis, MN 55455, USA

<sup>b</sup> Thermacore Inc., Lancaster, PA 17601, USA

## ARTICLE INFO

### Article history:

Received 23 March 2011  
Received in revised form  
29 December 2011  
Accepted 2 January 2012  
Available online 10 January 2012

### Keywords:

Piezoelectric actuator  
Oval loop  
Displacement amplification  
Translational motion  
Agitation

## ABSTRACT

Compact piezoelectric actuators based on an oval loop shell structure were fabricated and their vibration characteristics were investigated. The actuators can successfully create a translational motion at a high frequency and a large displacement working distance at the second resonant mode of the shell structure. As a result of a shot peening process to harden the surface and increase the strength of the shell structures, fatigue limits were enhanced. The highest operating frequency of 1444 Hz was achieved with about 1.5 mm translational displacement under an applied voltage of 100 VAC. The largest amplified displacement of 2.1 mm was obtained at a resonant frequency of 961 Hz. Displacement amplification ratios between static and resonance conditions are presented and compared. A theoretical approach was provided to estimate the natural frequencies of the oval loop shell actuators. The estimated natural frequencies of the actuators agreed with experimental values to within 12%. In addition, load bearing capacity and efficiency of one of the shell actuators was evaluated with an experimental method. The calculated actuator efficiency is around 55% when 3.1 g of mass is loaded to the actuator and an applied voltage of 140 V is applied. A possible application of the actuator, a cooling device, was demonstrated by providing its configuration and test results.

© 2012 Elsevier B.V. All rights reserved.

## 1. Introduction

Piezoelectric materials have been utilized in various applications such as micro/nano positioning devices, motors, sensors, actuators, etc. An attractive feature is its high energy density. The optimum actuator should be able to satisfy the criterion of high displacement, large force, broad range of operating frequency, and low electrical power consumption [1]. Even though many piezoelectric actuators have been developed in the past, it is difficult to find examples that achieved all the parameters of large mechanical stroke and force and high operating frequency at once. Piezoelectric bending actuators with either unimorph or bimorph piezoelectric ceramics attached to high elastic shim materials can generate flapping motions with sufficiently large displacements [2–5]. However, their blocking force is very small compare to other actuation techniques. Piezoelectric multi-layered stack actuators can provide a very large blocking force with an operating frequency extended to tens of kilohertz. Unfortunately, only an exceptionally small displacement of a few microns is obtained. Studies have been intensively performed to overcome the shortcoming of the stack actuator. A hydraulic displacement amplification can afford a long

augmented stroke and force but with moderately low operating frequencies of below a few hundred hertz [6–9]. The complexity of the mechanical components such as pumps, moving pistons, valves, etc. and reliability problems regarding leakage of liquid restrict the piezo hydraulic actuators to a narrow area of applications. Relatively large power consumption to achieve high dynamic actuation is another issue of the piezo hydraulic actuators. Many lever mechanisms such as moon- or cymbal-types were developed for displacement amplification [1]. Ham et al. [10] developed a piezoelectric pump using a hinge-lever amplification mechanism in order to magnify displacements of piezo stacks. They amplified the displacement up to 683  $\mu\text{m}$  from 28  $\mu\text{m}$ , the original displacement of the piezo stack, with an applied voltage of 100 V. The pump showed maximum capability at an operating frequency of 250 Hz. Joshi and Priya [11] proposed and fabricated an actuator design called the “piezo-bow” which consists of flexural metal caps attached to the piezo stack actuator through metal bars. The “piezo-bow” actuator exhibited about 20 times the amplification ratio, showed a high blocking force, and achieved high frequencies of about 2 kHz. Their amplified displacement was less than one mm. Ma et al. [12] proposed a bridge-type flexure hinge for displacement amplification. Numerical and theoretical studies were performed to analyze the ideal displacement amplification ratio of the bridge-type flexure hinge. Furukawa et al. [13] developed a flexure-hinged translation mechanism with a push and pull

\* Corresponding author. Tel.: +1 612 626 1636; fax: +1 612 625 6069.  
E-mail address: [tcui@me.umn.edu](mailto:tcui@me.umn.edu) (T. Cui).

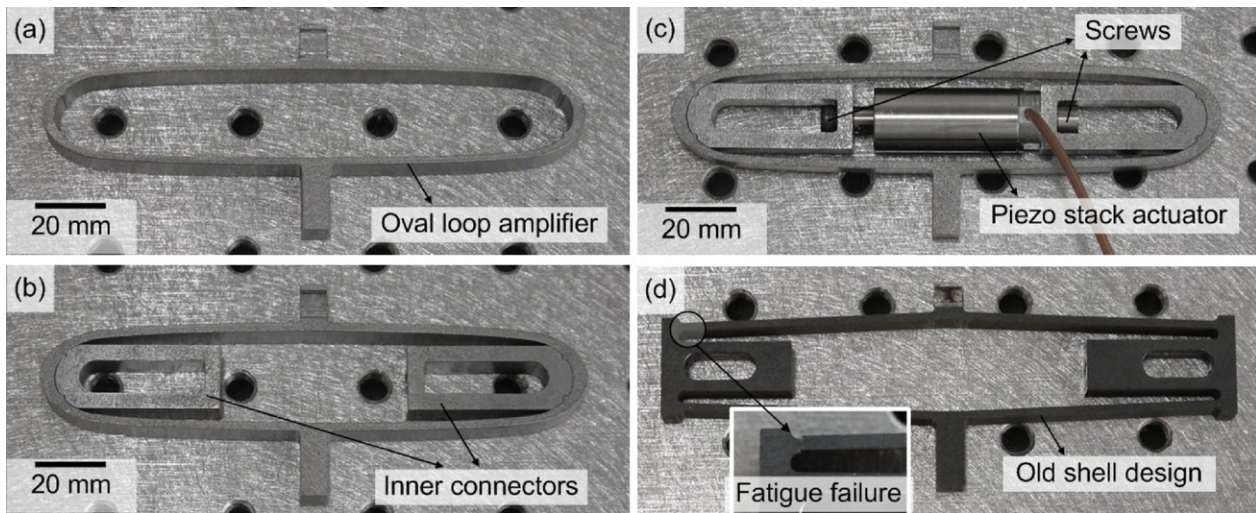


**Fig. 1.** (a) Oval loop amplifier, (b) oval loop amplifier attached with two inner connectors, (c) oval loop amplifier coupled with piezo stack actuator, and (d) old shell design cut as one piece including inner connector parts. Inset shows the fatigue failure point where the spatial expansion occurs.

driving system using two piezo stacks suitable for mechanical scanning stages with very high precision. The scanning range of  $60\ \mu\text{m}$  and a natural frequency of  $1175\ \text{Hz}$  were demonstrated with the given amplification system. Juuti et al. [14] proposed another bridge-type flexure hinge mechanism to amplify the displacement of the pre-stressed piezo disk actuator. In order to avoid fractures of levers, they applied a laminated two-layered structure cut by a laser. Their maximum amplified displacement was about  $1.2\ \text{mm}$  from  $50\ \mu\text{m}$  piezo displacement at an applied voltage of  $500\ \text{V}$ . However, their actuator is not suitable for high frequency application. Mulling et al. [15] studied load capabilities of a thin-layered unimorph actuator which is commercially available under the name THUNDER™. They revealed that end conditions and load capability have a significant effect on the performance of the actuator, interdependently. Kim et al. [16] developed a small-scale, three-dimensional, bridge-type flexure hinge mechanism with a maximum operating frequency and displacement of up to several kilohertz and a few hundred microns, respectively. Lam et al. [17] fabricated a cymbal type actuator with a lead-free piezo-ceramic disk. The actuator achieved very high fundamental resonance frequencies, above  $80\ \text{kHz}$ , with relatively low amplified displacements. Muraoka and Sanada [18] developed a honeycomb-like, successively connected, lever-hinge mechanism to amplify the displacement of piezo stack actuators. Neal and Asada [19] proposed a piezoelectric actuator that can provide one hundred times amplification using the buckling phenomenon of a flexure-based structure. Ueda et al. [20] developed a new strain amplification design with a nested-rhombus, multilayer system. The multi-layered actuator can generate 21% effective strain from the  $12\ \text{mm}$  actuator height which is  $2.53\ \text{mm}$ . However, this mechanism is not appropriate for high-frequency application.

In the present work, we proposed piezoelectric actuators with a high frequency of above  $1\ \text{kHz}$  and a large displacement in the mm range, with low power consumption of less than  $10\ \text{W}$ , based on an oval-shape loop shell structure. The purpose of this work is to address effective ways of amplifying the very small displacement of piezo stack actuators in highly dynamic actuation modes. CEDRAT Technologies has developed and commercialized a similar type of actuator using a loop shell structure with the name of APA (Amplified Piezoelectric Actuator) [21]. The APAs can gain an amplified stroke from several tens of microns to about  $1\ \text{mm}$ . However, their operating frequency is less than  $500\ \text{Hz}$  when the actuator generates the largest amplified stroke. When the actuators are operating at higher frequencies, above  $1\ \text{kHz}$ , the amplified stroke is limited

to tens of microns. The proposed actuator used in the present work can utilize the second resonance mode as well as the first mode to maximize the operating frequencies and amplified strokes at the same time. In this study, six different oval loop shell piezo actuators which exhibited several hundreds of amplification ratios at the first and second resonant modes with a moderate range of applied voltages, between  $20\ \text{V}$  and  $100\ \text{V}$ , were fabricated. The results are very promising and cannot be found in the literature.

## 2. Design and fabrication

A piezoelectric actuator with an oval loop shell amplifier is shown in Fig. 1. The oval loop shell (Fig. 1(a)) plays a role of amplifying a displacement from a piezo stack actuator. In order to connect the piezo stack actuator to the oval loop shell, two inner connectors are attached at the each inner side of the shell with epoxy (Fig. 1(b)). For an earlier design of the piezo actuator, two inner connectors and the outer shell were cut as one piece. However, due to the characteristics of high duty cycles of the actuator, a fatigue failure occurred within  $900,000$  cycles at the joint where a large area expansion exists. Thus, the inner connection parts were separated to give large curvature, minimizing stress concentration through the outer shell. The earlier design of the actuator and the fatigue failure point are shown in Fig. 1(d). In the oval loop shell, the piezo stack actuator should be aligned exactly on the symmetry line dividing the oval loop upper and lower regions. Therefore, screws were used to fix the stack actuator at the correct position between two inner connectors. The piezo stack actuator is pre-stressed by shortening the distance between two inner pieces to less than the length of the stack actuator. Without sufficient pre-stress distance, the actuator could not generate good performance as the actuation energy from the piezo stack actuator would not be fully transmitted to the oval loop shell structure. The pre-stress distance is around  $60\ \mu\text{m}$ . The oval loop shell and the inner pieces were fabricated by wire EDM (Electrical Discharge Machining) using 5160 spring steel. Such steel has been extensively used for spring applications, such as a leaf springs.

In order to achieve a high frequency of above  $1\ \text{kHz}$  and a large displacement of above the one mm range in an actuator with a low power consumption, it was desirable to use the structure's resonance modes. A schematic and the design parameters of the oval loop shell are presented in Fig. 2(a). The piezo stack actuator generates a translational displacement in the horizontal direction

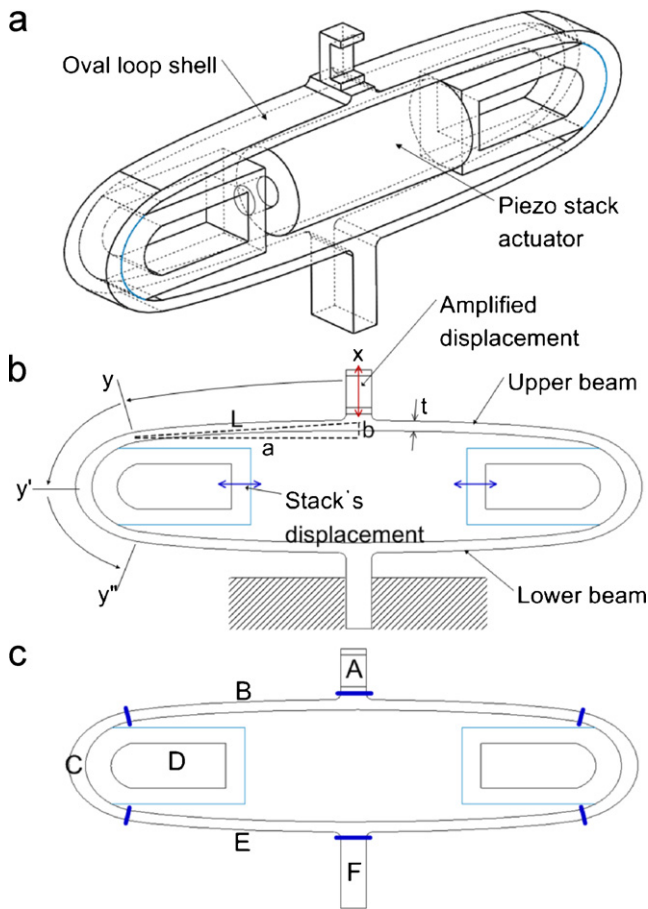


**Fig. 2.** (a) 3D view of the piezo actuator, (b) side view of oval loop shell and design parameters, and (c) various sections of the oval loop shell structure.

(horizontal arrows in Fig. 2(b)), and the oval loop shell amplifies the movement in the vertical direction (vertical arrow in Fig. 2(b)). The shell forms an oval-shaped closed loop with a uniform beam thickness ( $t$ ) between points  $x$  and  $y$ . To control and restrict bending motion within the section between  $x$  and  $y$ , the beam thickness was increased starting from  $y$  until it reaches  $y'$ . Next, it was decreased to the original thickness ( $t$ ) from  $y'$  to  $y''$ . In designing the oval loop shell, there are three parameters primarily to be considered to produce an amplified displacement and a high resonance frequency. They are next discussed. A right triangle could be drawn in

**Table 1**  
Six different oval loop shell designs fabricated for testing.

Oval loop shell type	$a$ (mm)	$b$ (mm)	$t$ (mm)
Shell 1	35	1.8	1.4
Shell 2	35	1.8	1.6
Shell 3	40	1.8	1.4
Shell 4	40	1.8	1.6
Shell 5	35	1.7	1.6
Shell 6	35	1.7	1.7

between vertices formed in the center and each end of the main beams (dashed lines in Fig. 2(b)). Two legs, ' $a$ ' and ' $b$ ' of the right triangle, are key design parameters as well as the beam thickness ' $t$ ,' an important parameter to affect the resonance frequency of the actuator.

One of the main design considerations is a size factor. Therefore, ' $a$ ' is selected to not exceed 50 mm so that the entire length of the actuator could be within 100 mm. As noted previously, the fatigue failure should be overcome because desired actuators have a characteristic of heavy duty cycles due to the high frequency and large displacement. Hence, in addition to the design modification, shot peening was applied onto the surface of the oval loop shells to induce compressive residual stresses in the shell structure. Literature shows that shot peening could enhance fatigue strength significantly. Grinspan and Gnanamoorthy [22] applied an oil jet peening process onto the surface of a carbon steel cantilever-type specimen. The peening process improved the fatigue strength about 19% compared to unpeened specimens. Aggarwall et al. [23] investigated the effect of the shot peening process for minimizing fretting fatigue failure of the spring steel leaf spring. In addition, other researchers employed shot peening to enhance fatigue strength of systems [24,25]. A shot-peened shell surface is shown in Fig. 3, compared with a normally machined 5160 spring steel surface. A specific test to measure lifetime was not performed. However, the modified and shot peened oval loop actuators were shown to withstand at least 18,000,000 cycles without a fatigue failure. Totally, six different oval loop shells were fabricated with different values of ' $a$ ,' ' $b$ ,' and ' $t$ ' in Fig. 2(b). The different design parameters of the oval loop shells are listed in Table 1. Shells 1 and 2 have the same ' $a$ ' and ' $b$ ' but different beam thicknesses of 1.4 mm and 1.6 mm. Shells 3 and 4 are longer than shells 1 and 2. Thus, among these four actuators we can examine effects of shell length and thickness on vibration characteristics at higher resonance modes of the structure. Shells 5 and 6 are selected mainly to see the effects of ' $b$ .' The Pst HD 200 piezo stack actuator from APC International, Ltd. was used for all the oval loop shells. Fig. 4 shows displacements of the

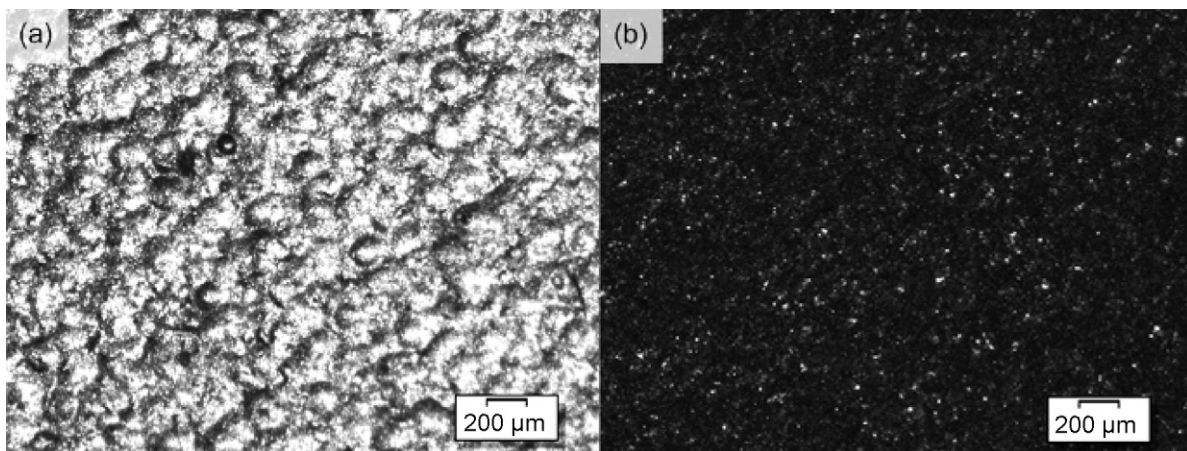


**Fig. 3.** (a) Shot peened shell surface and (b) bare surface of 5160 spring steel after the wire EDM process.

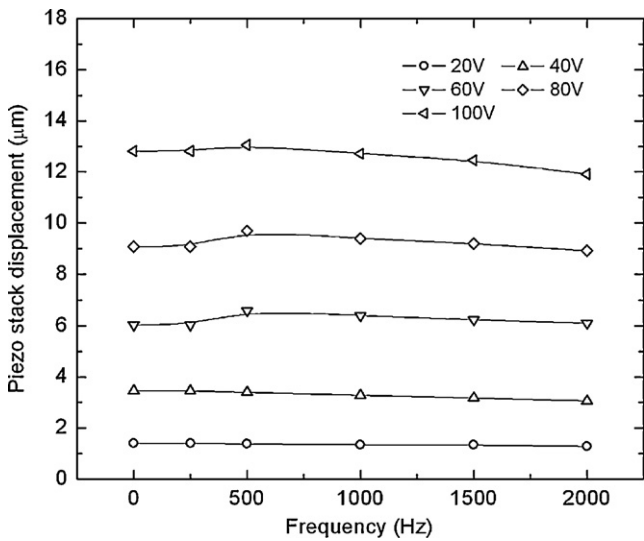


Fig. 4. The displacement of PSt HD 200 piezo stack actuator with different voltage and frequency.

stack actuator with different voltages and frequencies. The piezo stack actuator can generate fairly consistent displacements with a voltage below 100 VAC within the 2 kHz frequency range. However, with applied voltages above 100 VAC, the displacement decreases as the frequency exceeds 1 kHz. This is mainly due to insufficient current supply of the piezo amplifier used at higher frequencies and voltages. Therefore, a voltage below 100 VAC is regarded as a proper operating voltage for a given stack actuator in the current application.

3. Experiments and results

Vibration characteristics of six fabricated shells were investigated with the PSV-400 laser Doppler vibrometer from Polytec. The VF-500 linear piezoelectric amplifier from Dynamic Structures and Materials, LLC. was used to supply a high voltage to the piezo stack actuator. AC (alternative current) signals were generated by the AFG3102 function generator from Tektronix, Inc. The experimental set up to investigate vibration characteristics using the laser vibrometer is illustrated in Fig. 5. The piezoelectric oval loop shell actuator is vertically placed on an optical table clamped with a

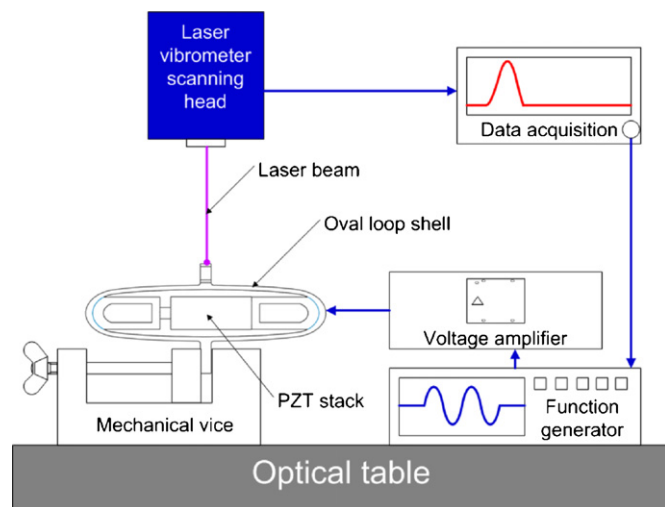


Fig. 5. Schematic of experimental facilities for measuring vibration characteristics of the actuators.

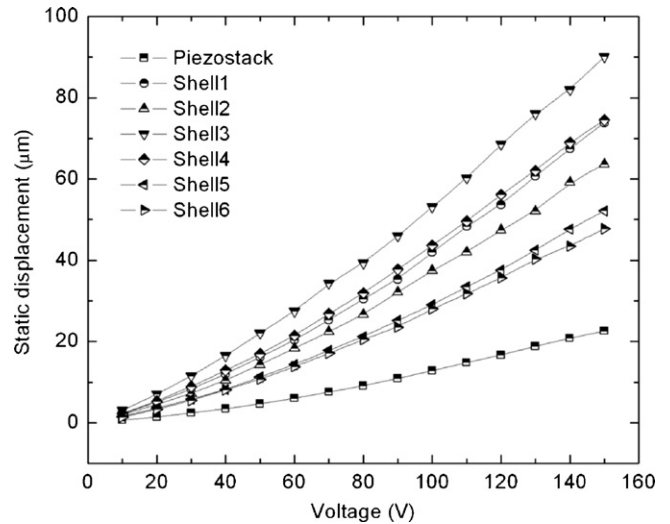


Fig. 6. The static deformation displacements of the shells compared with the displacements of the piezo stack actuator.

mechanical vice and a laser from the vibrometer head shoots on the upper surface of a rectangular bump in the center of the shell. Fig. 6 shows the displacements under a static deformation of the oval loop shells. It is apparent that the longer shells (shells 3 and 4) create larger displacements than the shorter shells (shells 1 and 2). Shell 3, with a thicker beam, has a larger static displacement than shell 4. The same pattern is seen between shells 1 and 2, which have only a thickness variation. Shell 5, with a decreased 'b' of 1.7 mm, produces a smaller static displacement, compared to shell 2. Shell 6 shows the minimum amplified static displacement among the six oval loop shell actuators because it is the smallest in size and the largest in beam thickness.

Fig. 7 presents displacement responses of six oval loop shells in the frequency domain. The response was scanned within a 2 kHz range since two appropriate resonance modes for translational displacement occur inside this frequency range. For all of the shells, two different resonance modes are shown (Fig. 7). The first mode of resonance frequencies is below 500 Hz. At the first mode, the lower beams in Fig. 2(b) oscillate, driving the entire shell structure, including the piezo stack actuator, in the vertical direction. In

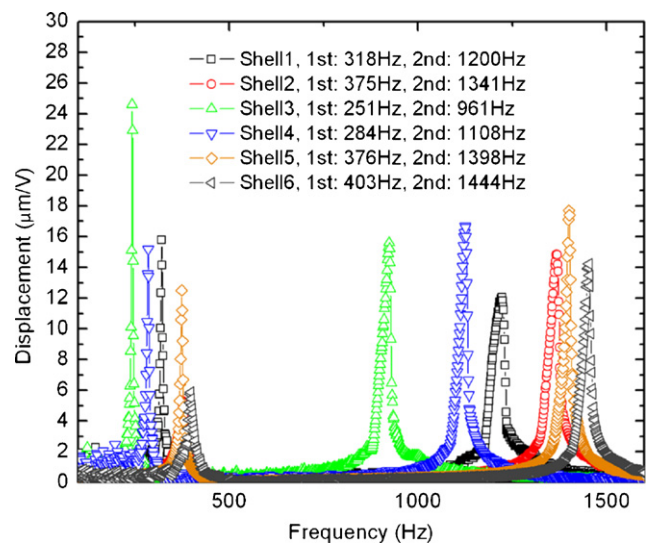


Fig. 7. The displacement response spectrum of six oval loop shells in the frequency domain from static to 2 kHz.

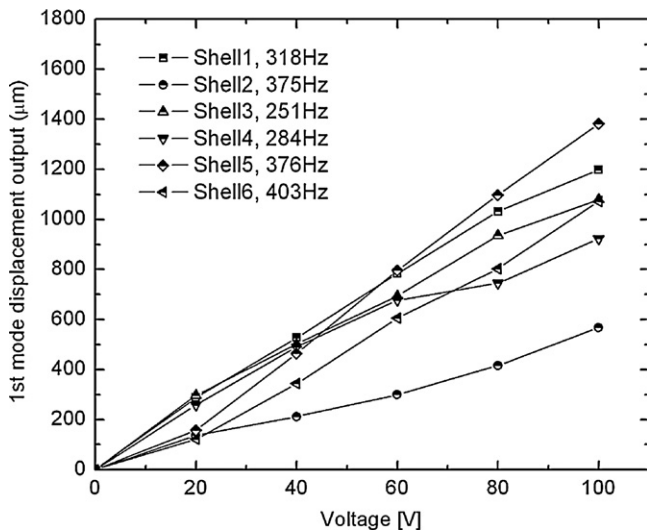


Fig. 8. The amplified displacements of six oval loop shells at the first mode of resonance.

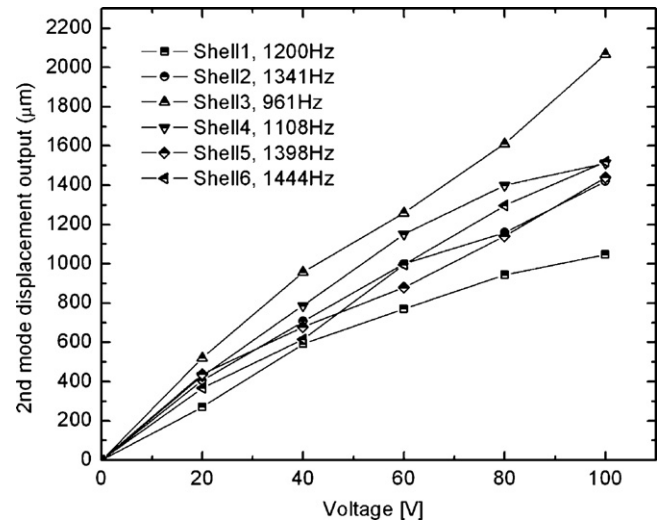


Fig. 9. The amplified displacements of six oval loop shells at the second mode of resonance.

this mode, it is not easy to support the whole body of the vibrating actuator, including the stack. At the second mode of the resonance, vibrational energy concentrates on the upper beams (Fig. 2(b)), and only the upper beams flap vigorously creating their translational displacement while the remainder of the actuator body remains stationary. From these results, we see that the resonance frequency rises as the thickness of the beams increases. Thus, shells 2 and 4 have larger resonance frequencies of the first and second modes than shells 1 and 3. Apparently, the resonance frequencies of the shorter loops (shells 1 and 2) are larger than the longer ones (shells 3 and 4). Shell 6 generates the highest resonance frequencies since the shell stiffness is largest, due to the shortest length and the thicker beam (1.7 mm).

Amplified displacements at the first mode of resonance of the shells are presented in Fig. 8 with different applied voltages between 0 and 100 VAC. For all the cases, the amplified displacements almost linearly increase with increasing voltages. Shell 3 shows the maximum amplified displacement of more than 1.6 mm at an applied voltage of 100 VAC. Surprisingly, shell 5 generated the second largest displacement at 100 VAC. It is shown that the pattern of the displacement amplification at the first resonance mode does not match the static amplification cases.

Fig. 9 represents the amplified displacements at the second mode of resonance. Again, shell 3 produced the largest displacement of more than 2 mm at a resonance frequency of 961 Hz. However, the resonance frequency is the smallest among the six oval loop shell actuators, due to its size being larger than the

other shells' sizes. Shell 4 shows the second largest displacement at a resonance frequency of 1108 Hz. Shell 6 achieved the highest resonance frequency of 1444 Hz with an amplified displacement of about 1.5 mm at an applied voltage of 100 VAC. All fabricated shells generated amplified displacements of more than 1 mm at the higher frequencies (above 1 kHz) except for shell 3, with a resonance frequency of 961 Hz. The performance of the oval loop shell piezo actuator is compared with other types of amplification mechanisms in the literature, in terms of the operating frequency and amplified displacement, in Table 2.

Fig. 10 shows amplification ratios of the shells, both at the static and resonance conditions, with comparison with the static case amplification ratio. At the static conditions (Fig. 10(a)), shell 3 can amplify the displacement up to 10 times at a lower voltage of 20 VAC. As the voltage increases, the amplification ratio decreases. This happens to all the cases and all six shells in the static and resonance conditions. At the first mode (Fig. 10(b)), shell 3 amplifies the displacement 213 times compared to the piezo stack actuator displacement at a voltage of 20 V. When 100 VAC is applied, the amplification ratio of shell 3 is 84. At the second mode (Fig. 10(c)), the amplification ratios improve over those of the first mode cases. At the applied voltage of 20 VAC, shell 3 magnifies the displacement 372 times from the displacement of the stack actuator. In addition, an amplification of 161 was achieved with an applied voltage of 100 VAC for shell 3. Shell 6, operating at the highest frequency of 1444 Hz, gives an amplification of 118 at 100 VAC.

In addition, the electrical power consumption data are presented in Fig. 11. The electrical power consumption depends on the

Table 2  
Performance comparison of the actuators in the literature.

	Amplification type	Frequency (Hz)	Amplified displacement (µm)
Present work (shell 6)	Flexural beam	1444	1519
Yoon and Washington [8]	Hydraulic	80	3180
Ham et al. [10]	Hinge-lever	250	683
Joshi and Priya [11]	Flexural cap	2000	15
Furukama et al. [13]	Flexure-hinge	1175	60
Juuti et al. [14]	Bridge	Static condition	1200
Mulling et al. [15]	THUNDER™	Static condition	410
Kim et al. [16]	Bridge	5700	294
Lam et al. [17]	Cymbal-type	9420	~1
Muraoka and Sanada [18]	Honeycomb link	355	410
Cedrat Technologies [25]	APA 1000XL	210	1050
	APA 100MML	1730	100

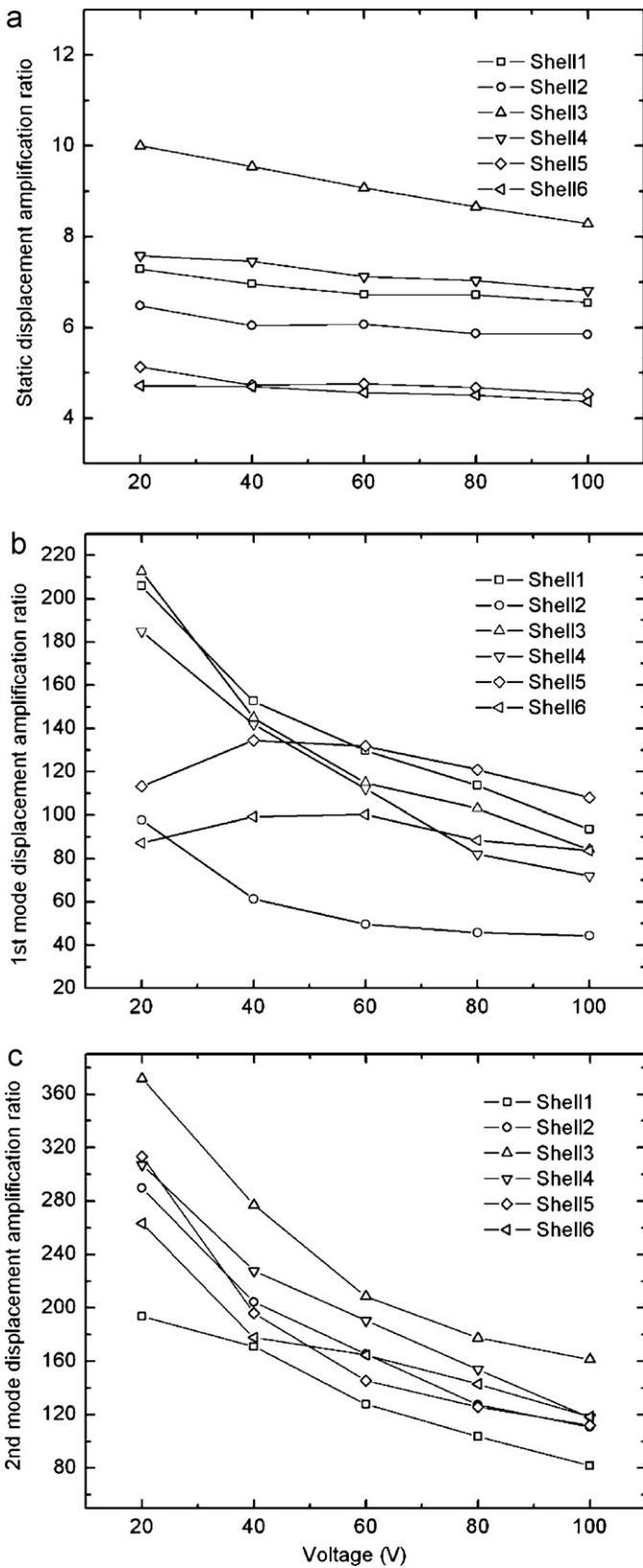


Fig. 10. Comparisons of amplification ratio at the static condition (a), the first mode (b), and the second mode (c).

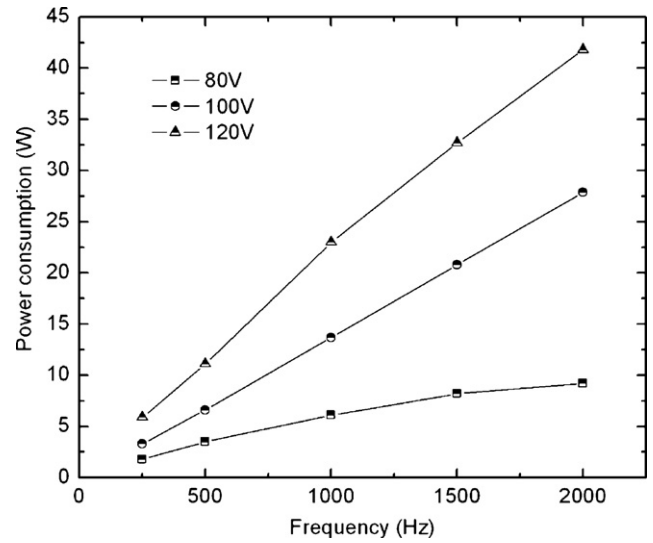


Fig. 11. Electrical power consumption of the piezo stack actuator.

performance of the piezo stack actuator. The power consumption was measured based on the following equation.

$$P_e = \frac{1}{T} \int_0^T V(t) \cdot I(t) dt \quad (1)$$

where  $T$  is the period over which data were measured. The varying voltage and current,  $V(t)$  and  $I(t)$ , are measured by a digital oscilloscope between the output of the piezoelectric amplifier and the input to the piezo stack actuator. The current to the piezo stack actuator was measured by placing a resistor of  $10 \Omega$  between the ground and the piezo stack actuator. The oscilloscope reads the voltage drop between the two junctions and the current to the stack actuator can be calculated by dividing the voltage drop with the resistance. The results show that the power consumption linearly increases with operating frequency of the stack actuator. At an applied voltage of 80 VAC, all the oval loop actuators can be operated with a power of less than 10 W. The amplified displacements and amplification ratios of the oval loop shell actuators at the applied voltage of 80 V are listed in Table 3. The power consumption, operating frequency, and voltage range can be controlled, considering the characteristics of applications.

#### 4. Natural frequency prediction

In the present report, predicting natural frequencies of the oval loop shell structure was attempted as the first step for theoretically evaluating dynamic characteristics of the actuator. A spring constant of the oval loop shell structure was evaluated in order to define the actuator system. It was treated as a simple one-degree-of-freedom spring-mass system. During the process, assumptions were made to simplify the analysis. First, air viscous damping

Table 3  
Amplified displacement and amplification ratio comparisons of the shells measured at 80 V.

	Amplified displacement ( $\mu\text{m}$ )		Amplification ratio	
	First mode	Second mode	First mode	Second mode
Shell 1	1032	944	114	104
Shell 2	416	1159	46	128
Shell 3	936	1612	103	177
Shell 4	745	1399	82	154
Shell 5	1098	1142	121	126
Shell 6	803	1298	88	143

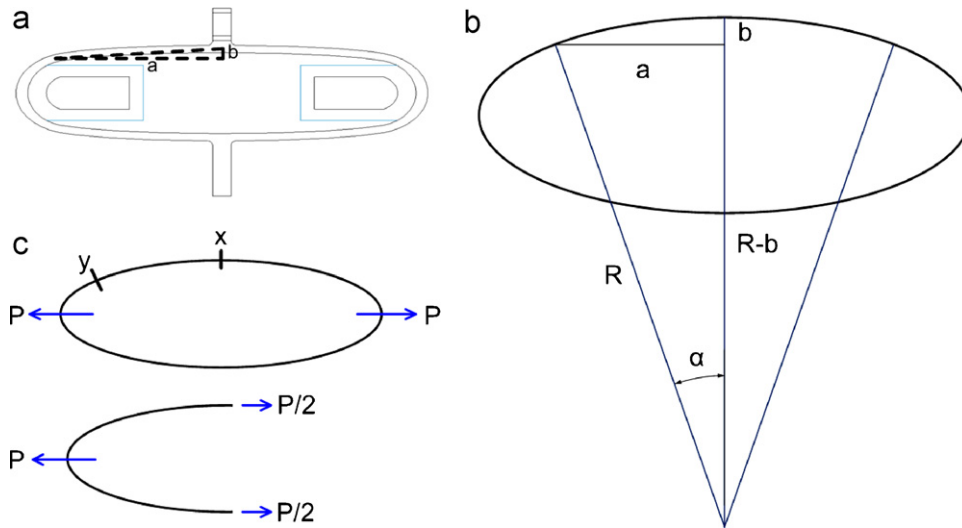


Fig. 12. (a) Oval loop shell with two design parameters ‘a’ and ‘b’, (b) radius of the oval loop beam, (c) freebody diagram with the applied force of, P, from the piezo stack actuator.

effects applied to the flapping beam surface were neglected. Second, nonlinear effects of the vibrating shell structure and the piezo stack actuator due to thermal dissipation from the piezo stack actuator at high dynamic actuation states were not counted. Third, it was assumed that flexural deformation of the beam is restricted in the section between  $x$  and  $y$  in Fig. 2(b). Finally, it was regarded that the spring constants of the upper and lower beams are identical, due to the symmetric shape of the oval loop shell. When the piezo stack actuator generates the force of  $2P$  stretching out the shell structure in the horizontal direction, the force is distributed to each horizontal direction. The freebody diagram of the oval loop shell structure, when cut along the central, vertical line of symmetry, is shown in Fig. 12(c). The flexural section of the beam (between  $x$  and  $y$ ) can be defined with an angle ‘ $\alpha$ ’ starting from the center of the shell ( $x$ ) and passing to the end of the flexural section ( $y$ ). In the flexural section, the shell structure has a constant radius of ‘ $R$ ’. Therefore, the relation between ‘a,’ ‘b,’ ‘ $\alpha$ ,’ and ‘ $R$ ’ can be expressed as:

$$\alpha = \tan^{-1} \left( \frac{a}{R-b} \right) \quad (2)$$

The spring constants of the shell structure in the vertical and horizontal directions can be calculated separately by the use of Castigliano’s theorem [26]. In the horizontal direction, the strain energy ( $U$ ) stored in the flexural section (between  $x$  and  $y$ ) can be expressed as:

$$U = \int_0^S \frac{M^2 ds}{2EI} = \int_0^\alpha \frac{M^2 R}{2EI} d\phi \quad (3)$$

where  $M$ ,  $S$ ,  $E$ , and  $I$  are moment, beam length of flexural section, modulus of elasticity, and moment of inertia, respectively. Therefore, the static horizontal displacement ( $\delta_h$ ) of the oval loop shell structure due to force,  $P$ , can be calculated as:

$$\delta_h = 4 \frac{dU}{dP} = \frac{4}{EI_z} \int_\beta^\alpha M \frac{dM}{dP} R d\phi \quad (4)$$

Herein, the flexural section of the beam is re-defined as a bump in the center of the oval loop shell structure (Fig. 2) is regarded as a rigid section. Thus, ‘ $\beta$ ’ indicates the actual starting angle of the flexural section next to the rigid bump in the center. A moment balance

calculation based on the left-side cross section of the flexural beam, shown in Fig. 13(b), is:

$$\sum M = -M + M_0 - \frac{P}{2}R + \frac{P}{2}R \cos \phi = 0 \quad (5)$$

therefore, the moment ( $M$ ) along the beam is:

$$M = M_0 - \frac{P}{2}R + \frac{P}{2}R \cos \phi \quad (6)$$

The initial moment ( $M_0$ ) applied at the center cross section of the beam due to the load,  $P$ , can be calculated when assuming that no rotation occurs at the center symmetry plane of the shell structure. Therefore, the following is valid:

$$\frac{dU}{dM_0} = \frac{1}{EI_z} \int_0^\alpha M \frac{dM}{dM_0} R d\phi = 0 \quad (7)$$

which leads the following:

$$\frac{dU}{dM_0} = \int_0^\alpha MR d\phi = 0 \left( \because \frac{dM}{dM_0} = 1 \right) \quad (8)$$

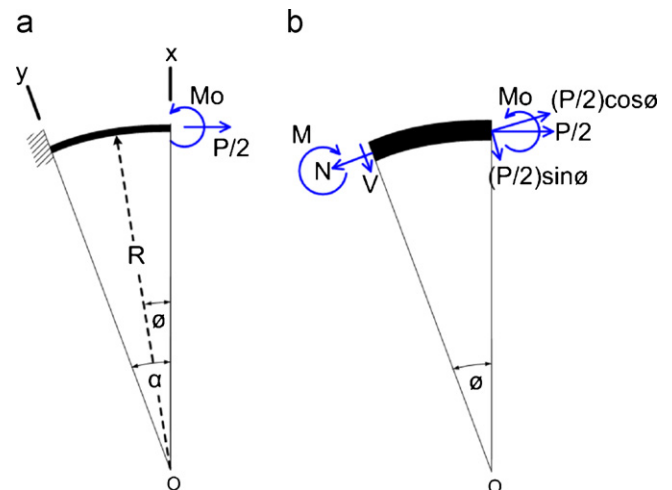


Fig. 13. Freebody diagrams of the flexural section of the oval loop shell.

**Table 4**  
Frequency comparisons between the experimental and analytical results.

	Experiment (Hz)		Theory (Hz)		Difference (%)	
	First mode	Second mode	First mode	Second mode	First mode	Second mode
Shell 1	318	1200	329	1101	3.3	−8.2
Shell 2	375	1341	387	1245	3.1	−7.2
Shell 3	251	961	271	886	8.0	−8.0
Shell 4	284	1108	318	1002	12.0	−12.3
Shell 5	376	1398	393	1236	4.4	−11.6
Shell 6	403	1444	423	1308	5.0	−9.4

After conducting the integration of Eq. (7), the expression for the initial moment applied at the center cross section becomes:

$$M_o = \frac{P}{2}R \left( 1 - \frac{\sin \alpha}{\alpha} \right) \quad (9)$$

Solving Eq. (4) with Eqs. (6) and (9), we find the horizontal displacement of the shell structure due to load,  $P$ , from the piezo stack actuator as:

$$\delta_h = \frac{PR^3}{EI_z} \left[ \frac{1}{2}\alpha + \frac{1}{4}\sin 2\alpha - \frac{\sin^2 \alpha}{\alpha} - \frac{1}{2}\beta - \frac{1}{4}\sin 2\beta - \frac{2\sin \alpha \sin \beta}{\alpha} + \frac{\sin^2 \alpha}{\alpha^2}\beta \right] \quad (10)$$

Therefore, the spring constant of either upper or lower beam in the horizontal direction is:

$$k_h = \frac{EI_z}{2R^3} \left[ \frac{1}{((1/2)\alpha + (1/4)\sin 2\alpha - (\sin^2 \alpha/\alpha) - (1/2)\beta - (1/4)\sin 2\beta - (2\sin \alpha \sin \beta/\alpha) + (\sin^2 \alpha/\alpha^2)\beta)} \right] \quad (11)$$

The spring constant in the vertical direction can be calculated by repeating the same process as done for the horizontal direction with the fictitious force  $Q$  applied in the vertical direction at the center of the shell structure. The calculated spring constant in the vertical direction is:

$$k_v = \frac{EI_z}{4R^3} \left[ \frac{1}{((1/4)\cos 2\alpha - (\sin \alpha \cos \alpha/\alpha) - (\sin \beta/\alpha) + (\sin \beta \cos \alpha/\alpha) + \beta(\sin \alpha/\alpha)(1 - \cos \alpha/\alpha) - (1/4)\cos 2\beta + (\sin \alpha \cos \beta/\alpha))} \right] \quad (12)$$

As will be discussed in the following sections, the oval loop shell structure has two different resonance modes within the 2 kHz frequency range. At the first mode, the lower beam vibrates, moving the entire actuator body up and down. On the other hand, only the upper beam flaps at the second mode. As two resonance modes were verified by experiments, herein, they were de-coupled and expressed as a single-degree-of-freedom, spring-mass system for each mode. The spring-mass system can be defined with the spring constant of the oval loop beam in the vertical direction and an appropriate effective lumped mass. Then, two natural frequencies of the oval loop shell structure can be estimated by the simple, well-known equation:

$$f_n = \frac{1}{2\pi} \sqrt{\frac{k_v}{M_{\text{eff}}}} \quad (13)$$

For the first mode, the effective lumped mass includes that of sections A–E, and the mass of the piezo stack actuator (Fig. 2(c)). For the second mode, the effective mass includes that of sections A and B. Results of a comparison between the estimated natural frequencies and the measured resonance frequencies of the oval loop shell actuator are listed in Table 4. The analytical calculations predict well two natural frequencies of the oval loop shell structures within an error of 13%. For the first mode, the analytical modeling over-predicts and shows the largest difference of 12% for shell 4. However, for the second mode, the analytical modeling under-predicts the frequencies compared with experimental values and also shows the largest error for shell 4.

## 5. Load capability and efficiency of the actuator

For completeness, an experimental investigation was performed about load capacity and efficiency of the actuator. Shell 3, with the PZT stack actuator P.010.40P from Physik Instrumente (PI) was utilized for the experiments. Load was gradually added by stacking carbon fiber plates on top of the actuator, and dynamic displacements and resonance frequencies at every step were measured with the laser vibrometer. Added mass starts from 3.1 g, which includes the supporting frame and one carbon fiber plate. From the results, it is confirmed that resonance frequency and dynamic displacement reduce as more load is applied to the actuator (Fig. 14). When around 49 g of mass was loaded to the actuator, the dynamic dis-

placement decayed to around 20  $\mu\text{m}$ . With more load, dynamic displacement becomes so weak that it is hard to distinguish it from the background noise. Therefore, this load point can be regarded as the maximum dynamic load to shell 3 at the applied voltage of 140

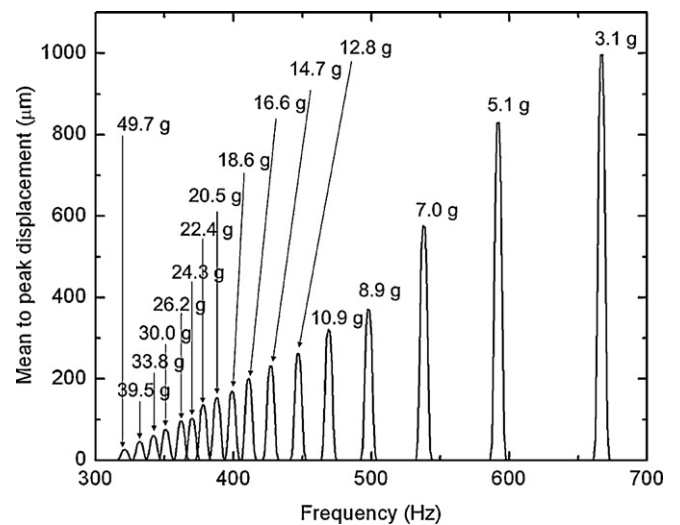


**Fig. 14.** Dynamic displacement and resonance frequency shift with different applied loads to shell 3.

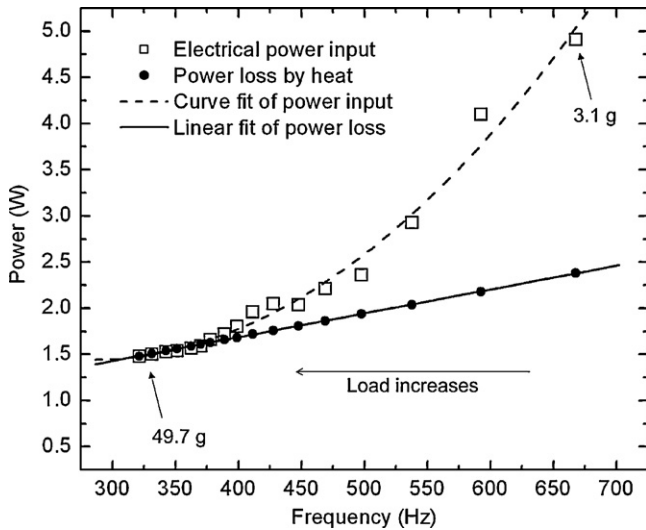


Fig. 15. Electrical power input and power loss by heat dissipation of the actuator with different applied loads and resonant frequencies.

VAC. Electrical power consumption of the actuator was also measured at every step of load addition. It is shown in Fig. 15. When the load addition is small, the decreasing rate of resonance frequency with added load is large and becomes smaller as more load is added to the actuator. Electrical power consumption is converging to a linear relation at the high load of around 50 g where very small dynamic displacements are generated. At these very low dynamic condition points, where the peak-to-peak displacements are less than 200 μm, it is assumed that almost all the electrical power input to the actuator is consumed as heat loss at the PZT stack. Furthermore, it is fortunate to know that heat loss of a piezo-actuator has a linear relation with an operating frequency [27]. Therefore, it is reasonable to estimate the heat loss at high dynamic conditions, based on this linear relation from the lower dynamic condition points. The extrapolation of the heat loss from the low dynamic points to the high dynamic points is shown in Fig. 15. As a result, the efficiency of the actuator could be defined as:

$$\eta(\%) = \frac{P_{\text{input}} - P_{\text{loss}}}{P_{\text{input}}} \times 100 \quad (14)$$

where  $P_{\text{input}}$  and  $P_{\text{loss}}$  are the electrical power input to the actuator and power loss by heat dissipation through the PZT stack actuator.

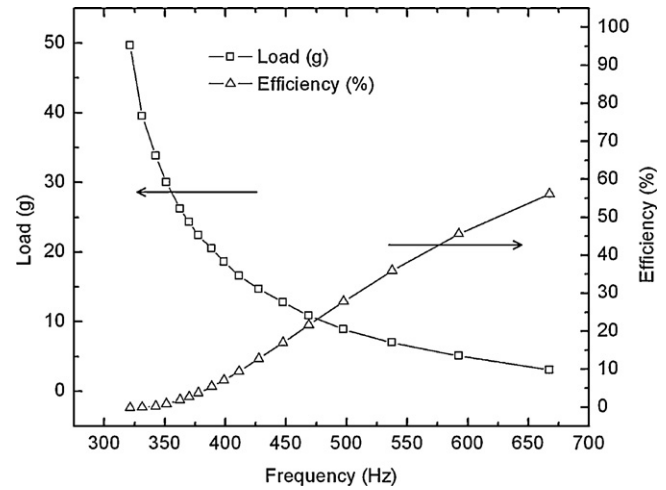


Fig. 16. Efficiency of the actuator shell 3 at different applied loads.

The numerator indicates the power consumed by the mechanical part of the oval loop actuator system. The calculated efficiencies of the actuator from the fit curves of electrical power input and heat loss are shown in Fig. 16. When 3.1 g of load is applied to the actuator, the efficiency is around 55%. The efficiency decreases to almost zero when 49.7 g of load is applied. Thus, the actuator generates almost no dynamic performance and all the electric power input at this condition is dissipated through heat loss of the PZT stack actuator.

### 6. Possible application

The oval loop shell piezo actuator can be utilized for applications where high dynamic actuation is required. A possible application example could be found in electronics cooling. The oval loop actuator can generate strong air currents with a light and stiff blade structure attached to the actuator playing the role of a translational fan for cooling heated electronic components. A simple test was performed to verify feasibility of the actuator as a translational fan. A rectangular blade (50 mm × 20 mm) made with a carbon fiber composite plate was attached to the center bump of the oval loop shell actuator (shell 3), as shown in Fig. 17(a). When the blade structure was attached to the actuator, the second resonance frequency of the actuator shifted from 961 Hz to 793 Hz due to the

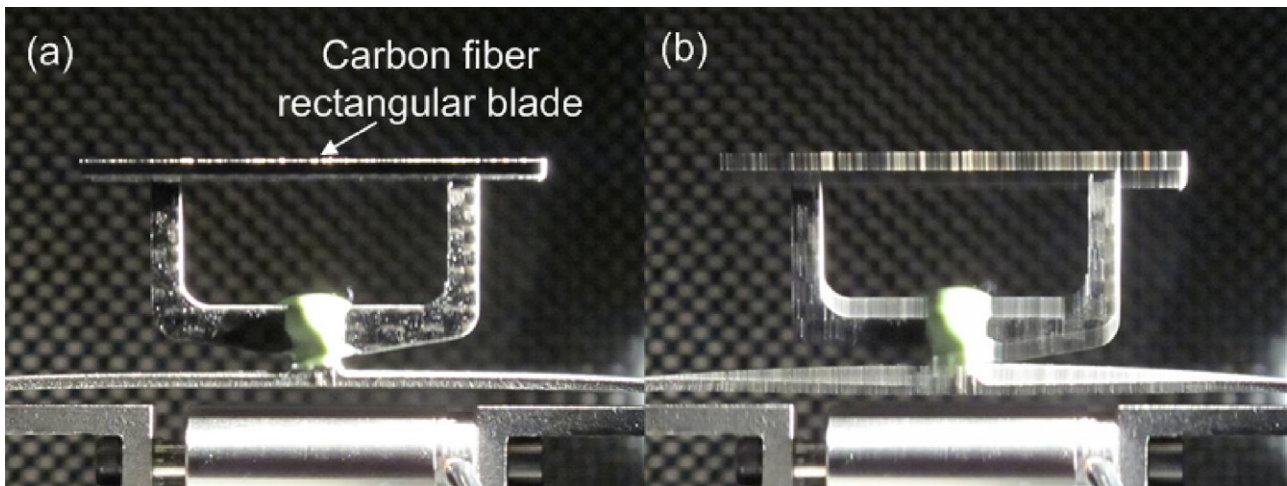


Fig. 17. (a) Oval loop shell piezo actuator (shell 3) with the carbon fiber blade attached on the top and (b) translational movement of the blade structure at the second resonance mode at 793 Hz shown by the fuzziness of the photo.

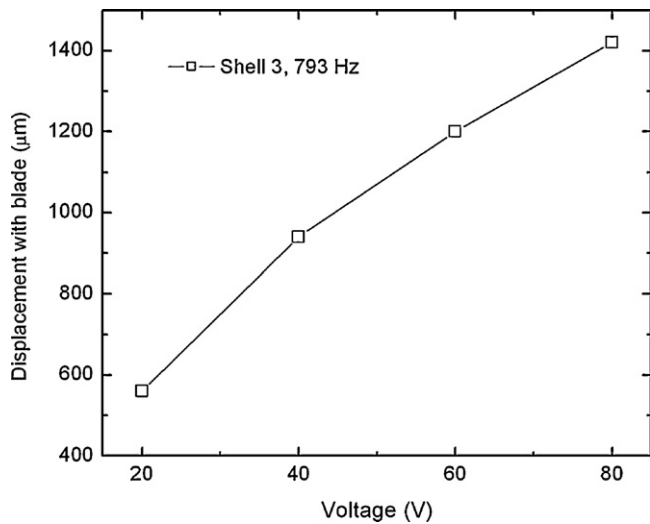


Fig. 18. Dynamic displacements of shell 1 with the blade structure at the second resonance mode.

increased mass. The translational motion of the oval loop shell actuator with the attached blade at the second resonance mode is shown in Fig. 17(b). The fuzziness of the picture shows the vibration amplitude. Displacements were measured with the laser vibrometer and shown in Fig. 18. The oval loop shell actuator (shell 3) with the blade generated a displacement of around 1.4 mm at 80 V. This is about 87% of the output displacement of the actuator operating without the blade structure. In addition to this application example, the oval loop shell actuator also might be utilized for driving a piston which produces flow to a synthetic jet [28–30], since the actuator can generate high dynamic translational motion. A synthetic jet is one in which flow departs a driven cavity, then reenters, giving a net zero mass flow; but, because half of the cycle is a jetting flow, it has many of the features of a continuous jet issuing out of the cavity.

## 7. Conclusions

The piezoelectric actuator with high frequency, large displacement, and low power consumption was successfully designed and fabricated based on the flexural oval loop shell structure. The shell amplifies the displacement of the piezo stack actuator and generates dynamic translational movement using resonant energy of the structure. In order to enhance fatigue strength of the actuator, shot peening was applied to the surfaces of the oval loop shells. After treatment, the fatigue strength was enhanced and the lifetime of the actuator increased significantly. At the second mode of resonance, the highest frequency achieved was 1444 Hz with an amplified displacement of around 1.5 mm when 100 VAC was applied to the actuator. The largest displacement of more than 2.0 mm was achieved with an operating frequency of 961 Hz. The theoretical solution was proposed to predict the natural frequencies of the oval loop shell actuator and showed a maximum error of around 12% compared to the results of experiments. The calculated actuator efficiency is around 50% when the minimal load of 3.1 g is applied to shell 3 with an applied voltage of 140 V. In addition to this, the possible application example of the actuator as a cooling device was provided with simple demonstration tests. The rectangular, thin carbon fiber plate was attached to the actuator driven by shell 3. The assembly generated around 1.4 mm of translational amplitude at an applied voltage of 80 V. The performance of the actuator is not restricted to the current design parameters in this paper. The operating conditions, such as the resonance

frequency and the amplified displacement, can be easily controlled to fulfill needs of specific applications by changing the design parameters. When more electrical power is available to the piezo stack actuator, higher displacement of dynamic actuation is possible. The current piezoelectric oval loop actuators can be utilized in applications where high-frequency translational movement with larger displacements is needed.

## Acknowledgements

This work was supported in part by the Defense Advanced Research Projects Agency (DARPA) MACE Program. The views expressed are those of the authors and do not reflect the official policy or position of the Department of Defense or the U.S. Government. Approved for Public Release, Distribution Unlimited.

## References

- [1] C. Niezrecki, D. Brei, S. Balakrishnan, A. Moskalik, Piezoelectric Actuation: State of the Art, *The Shock and Vibration Digest* 33 (2001) 269–280.
- [2] J.H. Yoo, J.I. Hong, W. Cao, Piezoelectric ceramic bimorph coupled to thin metal plate as cooling fan for electronic devices, *Sensors and Actuators A* 79 (2000) 8–12.
- [3] L.Q. Yao, J.G. Zhang, L. Lu, M.O. Lai, Nonlinear static characteristics of piezoelectric bending actuators under strong applied electric field, *Sensors and Actuators A* 115 (2004) 168–175.
- [4] J. Friend, A. Umeshima, T. Ishii, K. Nakamura, S. Ueha, A piezoelectric linear actuator formed from a multitude of bimorphs, *Sensors and Actuators A* 109 (2004) 242–251.
- [5] T. Acikalin, S.M. Wait, S.V. Garimella, A. Raman, Experimental investigation of the thermal performance of piezoelectric fans, *Heat Transfer Engineering* 25 (2004) 4–14.
- [6] C. Cadou, B. Zhang, Performance modeling of a piezo-hydraulic actuator, *Journal of Intelligent Material Systems and Structures* 14 (2003) 149–160.
- [7] J.E. Lindler, E.H. Anderson, M.E. Regelbrugge, Design and testing of piezoelectric-hydraulic actuators, in: *SPIE Smart Structures and Materials Symposium, Industrial and Commercial Applications of Smart Structures Technology*, San Diego, CA, USA, 2003, pp. 96–107.
- [8] H.S. Yoon, G. Washington, A millimeter-stroke piezoelectric hybrid actuator using hydraulic displacement amplification mechanism, in: *IEEE International Symposium on Industrial Electronics*, Montreal, Quebec, Canada, 2006, pp. 2809–2813.
- [9] J. Garcia-Bonito, M.J. Brennan, S.J. Elliott, A. David, A novel high-displacement piezoelectric actuator for active vibration control, *Smart Materials and Structures* 7 (1998) 31–42.
- [10] Y.B. Ham, W.S. Seo, W.Y. Cho, D.W. Yun, J.H. Park, S.N. Yun, Development of a piezoelectric pump using hinge-lever amplification mechanism, *Journal of Electroceramics* 23 (2009) 346–350.
- [11] M. Joshi, S. Priya, Piezo-bow: high displacement and high blocking force actuator, *Integrated Ferroelectrics* 82 (2006) 25–43.
- [12] H.W. Ma, S.M. Yao, L.Q. Wang, Z. Zhong, Analysis of the displacement amplification ratio of bridge-type flexure hinge, *Sensors and Actuators A* 132 (2006) 730–736.
- [13] E. Furukawa, M. Mizuno, T. Doi, Development of a flexure-hinged translational mechanism driven by two piezoelectric stacks, *JSME International Series C: Dynamics, Control, Robotics, Design and Manufacturing* 38 (1995) 743–748.
- [14] J. Juuti, K. Kordas, R. Lonnakko, V.-P. Moilanen, S. Leppavuori, Mechanically amplified large displacement piezoelectric actuators, *Sensors and Actuators A* 120 (2005) 225–231.
- [15] J. Mulling, T. Usher, B. Dessent, J. Ralmer, P. Franzone, E. Grant, A. Kingon, Load characterization of high displacement piezoelectric actuators with various end conditions, *Sensors and Actuators A* 94 (2001) 19–24.
- [16] J.H. Kim, S.H. Kim, Y.K. Kwak, Development and optimization of 3-D bridge-type hinge mechanisms, *Sensors and Actuators A* 116 (2004) 530–538.
- [17] K.H. Lam, X.X. Wang, H.L.W. Chan, Lead-free piezoceramic cymbal actuator, *Sensors and Actuators A* 125 (2006) 393–397.
- [18] M. Muraoka, S. Sanada, Displacement amplifier for piezoelectric actuator based on honeycomb link mechanism, *Sensors and Actuators A* 157 (2010) 84–90.
- [19] D. Neal, H.H. Asada, Dynamic performance of nonlinear 100× displacement amplification piezoelectric actuator, in: *ASME 2010 Dynamic Systems and Control Conference*, Cambridge, MA, USA, 2010, pp. 65–72.

- [20] J. Ueda, T.W. Secord, H.H. Asada, Large Effective-Strain Piezoelectric Actuators Using Nested Cellular Architecture With Exponential Strain Amplification Mechanisms, *IEEE/ASME Transactions on Mechatronics* 15 (2010) 770–782.
- [21] CEDRAT Technologies, 07/26/2011. <http://www.cedrat.com/en/mechatronic-products/actuators/apa.html>.
- [22] A.S. Grinspan, R. Gnanamoorthy, Effect of oil jet peening duration on surface modification and fatigue behavior of medium carbon steel, *AISI 1040, Materials Science and Engineering A* 456 (2007) 210–217.
- [23] M.L. Aggarwall, R.A. Khan, V.P. Agrawal, Investigation into the effects of shot peening on the fretting fatigue behavior of 65Si7 spring steel leaf springs, *Journal of Materials: Design and Applications* 219 (2004) 139–147.
- [24] H. Mano, S. Kondo, A. Matsumuro, Microstructured surface layer induced by shot peening and its effect on fatigue strength, *Transactions of Japan Society of Spring Engineers* 51 (2006).
- [25] V. Sabelkin, S.A. Martinez, S. Mall, S. Sathish, M.P. Blodgett, Effects of shot-peening intensity on fretting fatigue crack-initiation behaviour of Ti–6Al–4V, in: *Fatigue & Fracture of Engineering Materials & Structures*, Wiley-Blackwell, 2005, pp. 321–332.
- [26] S. Timoshenko, *Strength of Materials*, third ed., D. Van Nostrand Company, Inc., 1955.
- [27] T. Jordan, Z. Ounaies, J. Tripp, P. Tcheng, Electrical properties and power considerations of a piezoelectric actuator, in: *ICASE*, 2000.
- [28] A. Glezer, M. Amitay, Synthetic jets, *Annual Review of Fluid Mechanics* 34 (2002) 503–529.
- [29] Y. Zhou, B.-F. Wang, Research on fluidic dynamic characteristics of the piezoelectric synthetic jet actuator, *Journal of Intelligent Material Systems and Structures* 19 (2008) 351–357.
- [30] D. Jinjun, Y. Weizheng, L. Jian, S. Dandong, M. Binghe, Design and fabrication of a piezoelectric micro synthetic jet actuator, in: *Nano/Micro Engineered and Molecular Systems (NEMS)*, IEEE International Conference on, 2011, pp. 301–304.

## Biographies

**Taiho Yeom** is a Ph.D. student at the Mechanical Engineering Department of the University of Minnesota. He received his B.S. degree in mechanical engineering from Ajou University, Suwon, South Korea, in 2005 and M.S. degree in mechanical and aerospace engineering from Oklahoma State University, Stillwater, USA, in 2007. Currently, he is working on the MACE project developing piezoelectric flow agitators for electronics cooling.

**Terrence W. Simon** is a Professor of Mechanical Engineering, has been a member of the Heat Transfer Laboratory since 1980 and was the Director of the Thermodynamics and Heat Transfer Division of ME from 1997 to 2005. His research deals with transport in steady and unsteady, turbulent and transitional flows, including flows through porous media, and boiling heat transfer.

**Min Zhang** is a Postdoc at the Mechanical Engineering Department of the University of Minnesota. From 2006 to 2008, he worked as a Postdoc in Tsinghua University, China. He received his Ph.D. degree in mechanical engineering from Dalian University of Technology, Dalian, China, in 2006. He is working on the active cooling system in MACE project.

**Mark T. North** joined Thermacore in 1993 after completing his Ph.D. in Mechanical Engineering at Cornell University and is currently an Engineering Group Leader for R&D. He has over 20 years of experience in the development and application of heat pipe technology. He is currently an Associate Editor of the *Journal of Thermal Science Engineering and Applications* and has been a member of the ASME K-16 committee for over 10 years. Dr. North has published over 40 technical papers and holds 6 US patents.

**Tianhong Cui** is a Professor of Mechanical Engineering at the University of Minnesota. From 1995 to 2003, he held research or faculty positions at Tsinghua University, University of Minnesota, National Laboratory of Metrology in Japan, and Louisiana Tech University. He received his B.S. from Nanjing University of Aeronautics and Astronautics in 1991, and his Ph.D. with honors from Chinese Academy of Sciences in 1995. His research interests include MEMS/NEMS and nanotechnology.